The Role of Particle Morphology in Interfacial Energy Transfer in CdSe/CdS Heterostructure Nanocrystals

Nicholas J. Borys,[1] Manfred J. Walter,[1] Jing Huang,[2] Dmitri V. Talapin,[2,3] John M. Lupton[1,4]*

Nanoscale semiconductor heterostructures such as tetrapods can be used to mimic light-harvesting processes. We used single-particle light-harvesting action spectroscopy to probe the impact of particle morphology on energy transfer and carrier relaxation across a heterojunction. The generic form of an action spectrum [in our experiments, photoluminescence excitation (PLE) under absorption in CdS and emission from CdSe in nanocrystal tetrapods, rods, and spheres] was controlled by the physical shape and resulting morphological variation in the quantum confinement parameters of the nanoparticle. A correlation between single-particle PLE and physical shape as determined by scanning electron microscopy was demonstrated. Such an analysis links local structural non-uniformities such as CdS bulbs forming around the CdSe core in CdSe/CdS nanorods to a lower probability of manifesting excitation energy–dependent emission spectra, which in turn is probably related to band alignment and electron delocalization at the heterojunction interface.

Advances in the synthesis of semiconductor nanoparticles have enabled exquisite control over composition and shape, yielding spherical, linear (*1*, *2*), and branched structures such as tetrapods (*3*–*5*). Although many semiconductor nanoparticles originally consisted of only one material, further opportunities for tailoring electronic functionalities are anticipated from nanoscale semiconductor heterostructures combining two or more materials (*5*). Indeed, a host of applications has emerged from precise control over nanostructure functionality, ranging from photovoltaics (*2*, *6*) to commercial light-emitting devices. A microscopic understanding of the migration of excitation energy in heterojunctions and the resulting interfacial charge transfer (*7*) is particularly important in developing photocatalytic compounds to split water (*8*) or reduce CO_2 (*9*). Due to only a slight mismatch in the lattice constants of the two materials, yet well-contrasted band gaps, the CdSe/CdS heterostructure has evolved as one of the workhorses for relating nanoparticle synthesis and shape to spectroscopic properties. Here we describe an optical classification of the quantum confinement in complex CdSe/CdS core/shell nanostructures by means of single-particle light-harvesting action spectroscopy, a versatile noncontact tool to measure electron transport or energy transfer on mesoscopic length scales (*10*). For a variety of nanostructure shapes, we probed the photoluminescence excitation (PLE) of the absorbing CdS through emission from the lower-gap CdSe. We identified two distinct categories of action spectra, characteristic of the physical shape and quantum confinement parameters of the semiconductor heterostructures, and showed how the energetic landscape can inhibit complete electron transfer across the CdSe/CdS interface. This single-particle classification highlights the sensitivity of ensemble performance, such as in light-harvesting, to morphological characteristics that affect the intrinsic nature of the interfaces, thereby suggesting routes to future synthetic optimization.

Large optical absorption cross sections, enhanced stability, high quantum yields, and size-tunable electronic structure make semiconductor nanocrystals particularly interesting for light-harvesting and energy conversion applications (*2*, *6*). Nevertheless, there is still no clear consensus on the microscopic nature of interfacial energy levels and the process of carrier migration from one semiconductor to another. Very similar CdSe/CdS nanostructures can exhibit properties of either a type I heterostructure, in which both electron and positively charged hole are confined to one material, or a type II heterostructure, in which electron and hole separate between the materials (*11*–*14*). Naturally, such a distinction is crucial to choosing the correct material for a particular application: Light emission requires type I junctions, whereas charge separation in photovoltaics requires type II (*13*). Such knowledge of the interface is crucial for designing nanoparticle superstructures, such as inorganic dendrimers with a treelike branched architecture, with superior light-harvesting properties. A first step to such a structure is the heterojunction tetrapod (*5*).

Semiconductor nanoparticles are well suited to microscopic optical studies, which have revealed a surprising diversity in electronic properties between particles that are typically masked in ensemble-level measurements (*15*). Htoon *et al.*, for example, uncovered both discrete excitonic states and a quasi-continuum in the core of spherical CdSe particles capped with a ZnS shell (*16*). We probed energetic relaxation in individual CdSe/CdS nanoheterostructures of different shapes after optical excitation of the higher-gap CdS. This approach, leveraging single-particle PLE over a wide spectral range, illuminates the nature of both the high-gap material absorption and the subsequent intraparticle relaxation pro-

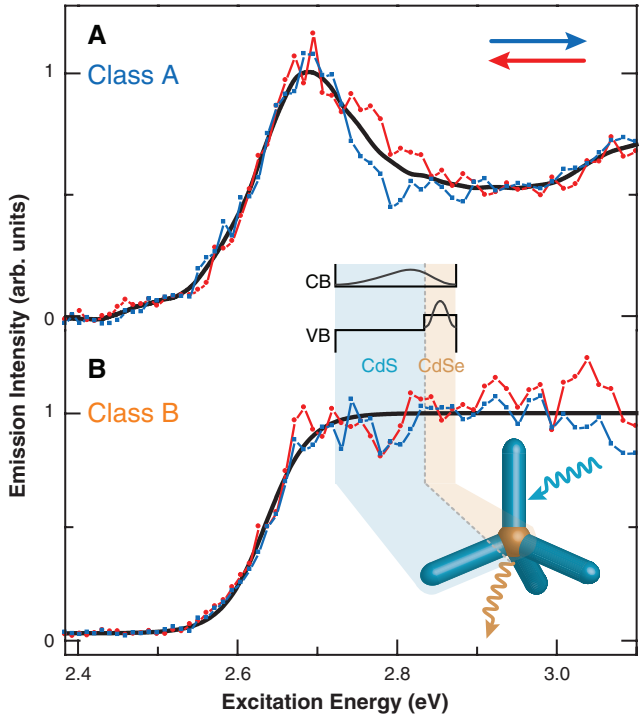

Fig. 1. Light-harvesting action spectroscopy at 4 K of two single semiconductor tetrapods consisting of a low-gap CdSe core and high-gap CdS arms. The nanoparticles are excited primarily above the CdS absorption edge, and emission is detected from the CdSe core. A sketch of the assumed electron and hole probability density distribution within the electronic band structure is shown in the inset in the middle. (**A**) For the first particle, the onset of absorption from the quantum-confined CdS exciton gives rise to a distinct peak that is then followed by absorption into a continuum of states at higher energy (red, scan downward in energy; blue, scan upward). (**B**) For the second particle, the peak associated with the CdS exciton is not present, and the spectrum is marked by a continuum of states after the onset of CdS absorption (the black lines are a guide to the eye).

[1]Department of Physics and Astronomy, University of Utah, Salt Lake City, UT 84112–0830, USA. [2]Department of Chemistry, University of Chicago, Chicago, IL 60637, USA. [3]Center for Nanoscale Materials, Argonne National Laboratory, Argonne, IL 60439, USA. [4]Institut für Experimentelle und Angewandte Physik, Universität Regensburg, D-93040 Regensburg, Germany.

*To whom correspondence should be addressed. E-mail: john.lupton@physik.uni-regensburg.de

cess, which are both ultimately crucial in designing light-harvesting applications (*6*). In contrast, most single-quantum–structure PLE spectroscopy (*16*–*18*) to date has been carried out over relatively narrow spectral ranges to probe distinct excitonic features, or else has analyzed excitation enhancement by metal nanoparticles at discrete wavelengths (*19*).

We focused our attention on CdSe/CdS tetrapods, which are inorganic light-harvesting complexes with very large absorption cross sections, which make them easily visible in single-particle measurements. A schematic of a CdSe/CdS tetrapod nanoparticle and a suggestive band diagram (*20*) are shown in the inset of Fig. 1. The structures consist of a CdSe core approximately 4 nm in diameter, which is surrounded by an antenna-like CdS shell. The shell has four arms that are 20 nm in length and 6 nm in diameter. We purified the tetrapod solution to an ensemble composition of at least 90% tetrapods, which appeared to be geometrically uniform in transmission electron microscopy (TEM) (*5*, *21*). Previous comparisons of theory and experiment have indicated that, on average, the CdSe/CdS interface should form a quasi–type II heterostructure, with an excited electron delocalizing over the CdSe and CdS conduction bands and the associated hole localizing on the lower-gap CdSe core (*14*). Initial studies on the tetrapods have suggested a similar electronic structure (*20*), although the energy offsets are such that a range of interfacial localization phenomena is conceivable (*13*): It is not straightforward to extrapolate band diagrams derived from bulk material parameters to solution-grown nanostructures. For these heterostructures, at energies above the CdS fundamental absorption edge, the CdS extinction dwarfs that of the CdSe, thus resulting in an absorption spectrum dominated by the CdS. The electronic structure, on the other hand, yields a luminescence spectrum arising from recombination in CdSe (*5*, *21*). The similarity of the ensemble nanoparticle PLE and absorption spectra indicates that this light-harvesting process is highly efficient (*5*). We expect the prominent onset of the PLE to correspond with the quantum-confined exciton of the CdS, followed by the typical continuum of higher energy states.

Such behavior was indeed observed in single-particle light-harvesting action at 4 K in Fig. 1A. We recorded the CdSe emission intensity while sweeping the laser excitation both down and up in energy (*22*). The particle exhibited a clear peak in the CdS absorption that can be attributed to the quantum-confined excitonic transition (*23*, *24*). We refer to PLE spectra with such behavior as class A. A second single tetrapod showed strikingly different behavior depicted in Fig. 1B, revealing particle-to-particle variations that are masked in ensemble measurements. In this case, there is no clear peak after the CdS absorption onset. We term these PLE spectra class B. Both classes were repeatedly observed in spatial proximity during the same excitation scan.

Although the tetrapods perform the desired light-harvesting function, they do not offer the best system in which to search for structural origins of the distinct PLE classification. We therefore used two further model systems to study the influence of particle form on PLE: nanorods,

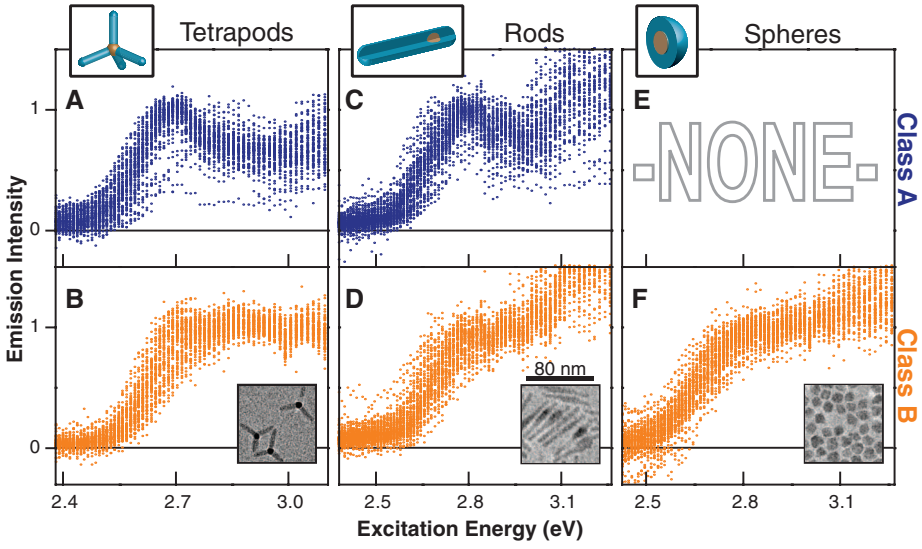

Fig. 2. Classification of single-particle light-harvesting action spectra for tetrapod, rod, and near-spherical nanoheterostructures. A total of 150, 150, and 75 raw spectra for tetrapods, rods, and spheres, respectively, are sorted into two groups. All curves are normalized to the CdS absorption onset intensity but are otherwise not manipulated. (**A** and **B**) 75 class A and 75 class B single-particle PLE spectra from tetrapod structures. (**C** and **D**) 75 class A and 75 class B single-particle PLE spectra from rod structures. (**E** and **F**) The near-sperical structures show only class B single-particle PLE spectra. Inset in (B) to (F) are representative TEM images of the tetrapods, rods, and spheres. Although the tetrapods appear uniform, the rod ensemble manifests two morphologies: one with a uniform diameter and the other with a pronounced bulb feature. The near-sperical structures are non-uniform in their deviations from isotropy.

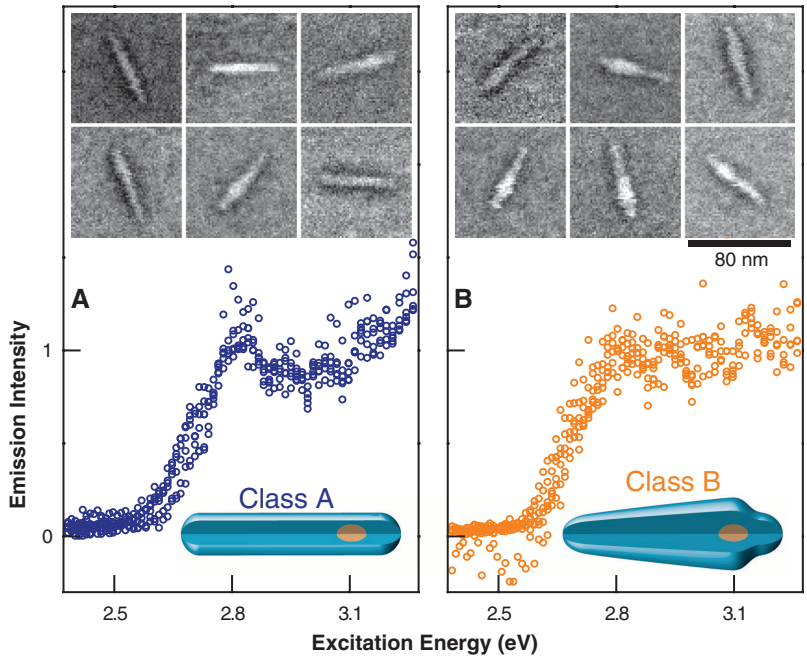

Fig. 3. Correlated SEM and PLE spectra of 12 single CdSe/CdS nanorods. (**A**) Six class A PLE spectra normalized to the CdS onset and plotted together with their corresponding SEM images, representative of rods with a uniform diameter (cartoon at bottom). (**B**) The SEM images of six rods that exhibit a class B PLE spectrum indicate that the spectral shape is attributable to rods that have a pronounced bulb feature and non-uniform diameter as sketched schematically in the cartoon. All correlated image-PLE pairs were chosen solely on the basis of the quality of the PLE spectrum, without any knowledge of the corresponding SEM image.

which mimic one arm and the core of the tetrapod; and nanospheres with a thick CdS shell. All structures had a similar CdSe core that was 4 nm in diameter. Figure 2 shows single-particle spectra of 150 tetrapod, 150 rod, and 75 near-spherical nanoheterostructures, normalized to the CdS absorption onset. Representative TEM images for each nanostructure are shown in the lower insets. The rods consist of a CdS arm 60 nm in length and approximately 6 nm in diameter surrounding the CdSe core. TEM indicated that the sample contained two general shapes of rods: rods that have a constant diameter over their length and those that have a bulb feature surrounding the CdSe core, resulting in a non-uniform rod diameter (*11*, *21*). Finally, the CdS shell for the near-spherical structures was a 4-nm-thick layer surrounding the CdSe core. TEM of these particles revealed that the thick CdS shell results in a non-uniform distribution of particles with anisotropic deviations from a perfect sphere. For the tetrapods and rods, each single-particle PLE spectrum can generally be categorized as class A (Fig. 2, A and C, respectively) or class B (Fig. 2, B and D, respectively). In contrast, we observed exclusively class B spectra for the near-spherical structures (Fig. 2F). We conclude that the origin of the different classes is not found in the combination of constituent materials but is related to the shape of the nanocrystal, which determines the symmetry of the confinement potential. Other approaches to representing the raw data, along with quantitative thresholds for differentiating between the two classes, are discussed in figs. S3 and S4 (*22*).

Through its relation to the quantum confinement effect, physical shape plays a crucial role in the optical and electronic properties of semiconductor nanocrystals (*13*, *23*, *25*). For the rods, where quantum confinement in the CdS is influenced mostly by diameter (*26*), the bulb structures consist of a range of diameters that will smear out the excitonic transition and will likely lead to particles with a class B spectrum. The same effect of shape variations in the direction of radial quantum confinement could also give rise to exclusively class B spectra in the near-spherical particles. In addition, quantum confinement in absorption in these particles may be weaker as the larger particle diameters approach the Bohr exciton radius in CdS, thus reducing the visibility of excitonic transitions.

To verify the role that shape plays in the PLE spectrum of a single nanocrystal, we correlated PLE measurements with scanning electron microscopy (SEM) of single rods. The correlation process is discussed in the text accompanying figs. S6 and S7. Figure 3 shows 12 PLE spectra and the SEM images of the corresponding nanorods. The pairs were selected solely on the basis of the quality of the PLE spectrum over up and down sweeps without any knowledge of the corresponding image. Figure 3A shows six class A PLE spectra normalized and plotted together; Fig. 3B shows six class B spectra. Inset in the plot are the corresponding SEM images. A clear trend that confirms the shape hypothesis is observable: All of the rods in Fig. 3A exhibit a class A PLE spectrum, and five out of six have a uniform diameter over the length of the rod. On the other hand, in Fig. 3B, all of the rods exhibit a class B PLE spectrum and have a pronounced bulb feature as anticipated (see the text accompanying fig. S7 for a discussion of the geometric thresholds invoked). These observations are consistent with single-particle PL (fig. S8), which demonstrates that rods with a class A PLE spectrum have higher-energy residual CdS emission due to their smaller diameters (stronger quantum confinement) than rods with a class B PLE spectrum. The basic statistical analysis presented in table S1 indicates that the probability of the results in Fig. 3 occurring by chance is 0.3%.

The similarity in PLE and emission spectra of rods, spheres, and tetrapods suggests that excessive CdS growth around the core could be responsible for the formation of two distinct spectroscopic classes of tetrapods. In addition, variations in effective arm diameter within a single tetrapod (*20*) or, quite generally, variations in

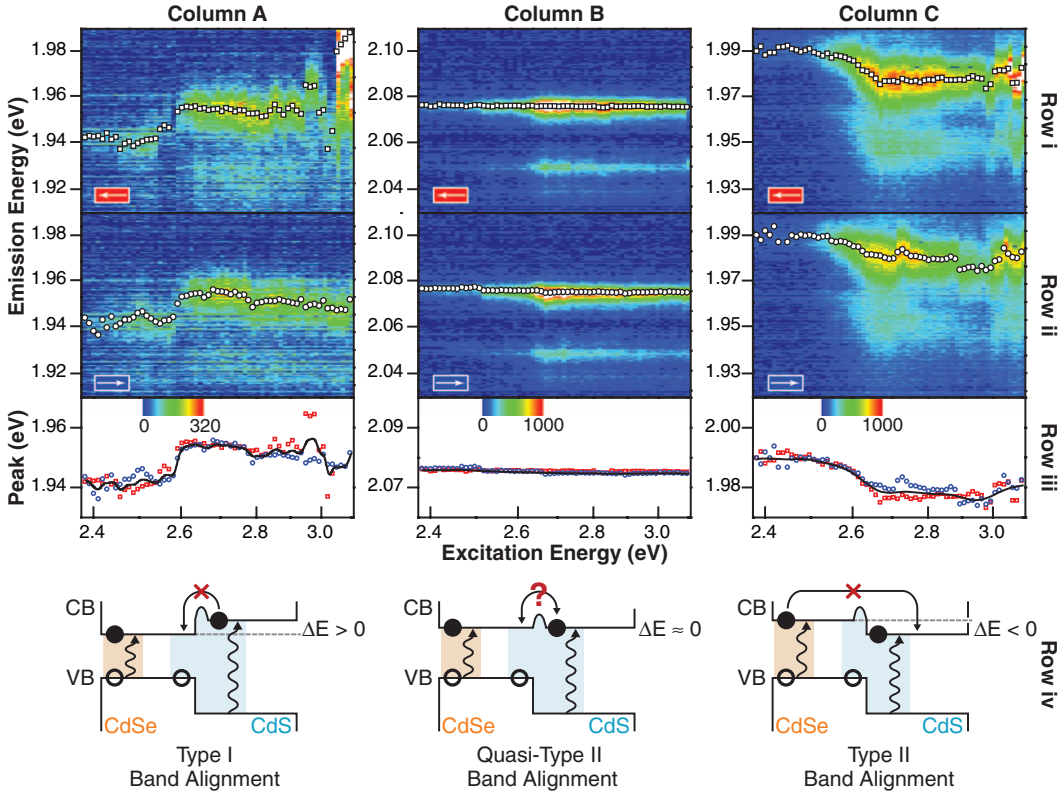

Fig. 4. Single-particle emission spectra as a function of excitation energy for three individual class A tetrapods, revealing the possible band alignment schemes. (**Column A**) The emission spectrum shifts to higher energies as the excitation energy is raised. Two-dimensional plots of emission as a function of excitation are shown for the laser sweep downward (Row i) and upward (Row ii) in energy. The main emission peak energy, extracted by fitting two Gaussians to the emission spectrum, is overlaid as white circles. (Row iii) The peak position as a function of excitation energy shows a steplike shift of ~10 meV close to the absorption onset of CdS at 2.6 eV. (Row iv) This situation can be rationalized in terms of a type I band alignment, where a barrier to thermalization of the electron from the CdS to the CdSe exists. Below 2.6 eV, direct excitation of the CdSe core occurs, whereas emission at higher excitation energies results from an interfacial exciton. (**Column B**) No spectral shift is seen with excitation energy, suggesting a quasi–type II band alignment. By analogy to column A, it is conceivable that a barrier to electron transfer between CdS and CdSe also exists due to, for example, lattice strain. (**Column C**) The type II band alignment is characterized by a shift of emission to lower energies as the excitation energy is raised from absorption in the CdSe core to the CdS shell. A barrier to electron transfer from CdSe to CdS must exist to prevent the core electron from transferring to the shell under excitation of the core. The black lines in the peak position plots are smoothed averages that serve as a guide for the eye.

intraparticle CdS-CdSe coupling strength that disrupt the particle symmetry, could lead to a loss of excitonic structure in PLE. We therefore propose that the single-particle PLE can serve as a predictor of particle morphology and indeed provides insight into the tetrapod shape, which is hard to obtain by other means.

Bulblike particle morphologies probably have featureless PLE spectra because the CdS shell is not defined by one fixed diameter, and therefore a range of excitonic transition energies exists. This morphological disorder within a single particle also appears to affect band alignment within the heterojunction, as revealed by spectrally resolving tetrapod emission as a function of excitation energy for 50 single tetrapods. Of these tetrapods, 26% [13 tetrapods (fig. S9)] showed a surprising dependence of the tetrapod emission energy on the excitation energy. Three such cases are detailed in Fig. 4.

The particle in column A of Fig. 4 exhibits a shift in emission to higher energy as the excitation energy is raised, although the shape of the emission spectrum remains characterized by the CdSe electronic transition and its phonon sideband. It is important to consider both sweep directions of the exciting laser because nanocrystals exhibit random spectral diffusion (*27*); the spectral changes are reversible upon downward (row i) and upward (row ii) sweeps. Row iii of column A plots the PL peak energy, which shows a distinct jump at an excitation energy of 2.6 eV. The position of the spectral jump corresponds to the onset of CdS absorption at 4 K and indicates a transition from direct excitation of the CdSe core to excitation of the CdS arm and subsequent relaxation to the CdSe. In contrast, the particle in column B exhibits emission independent of excitation. This case would be expected for a semiconductor heterostructure in which the high-energy electron-hole pair formed in the wide-gap semiconductor (CdS) relaxes down to the narrower-gap CdSe. Finally, in column C, the emission energy decreases with increasing excitation energy. As in column A, a change in the emission peak is observed around excitation at 2.6 eV.

To rationalize these observations, we consider the subtleties of conduction and valence band offsets between CdSe and CdS in row iv of Fig. 4. Studies of CdSe/CdS nanoparticles at the ensemble level have suggested that the CdSe valence band is consistently higher in energy than that of the CdS, although the conduction band alignment of the two materials is sensitive to nanoparticle geometry and may result in a type I, type II, or quasi–type II electronic structure (see sketches in Fig. 4 for definition) (*11*–*13*). Such band offsets will affect the emission spectrum if a barrier in the conduction band inhibits electron transfer between CdS and CdSe, which is conceivable given the interfacial strain due to the lattice mismatch of the two materials (*28*). We propose that the tetrapods in columns A and C of Fig. 4 are characterized by conduction band offsets ΔE, so that at least two distinct exciton states exist: CdSe core excitons and CdSe/CdS interfacial excitons. Because both states are emissive and hence stable, an interfacial barrier must be present, which prevents complete electron transfer to the lowest state in the conduction band, thereby impeding thermalization of the emissive exciton. A barrier to electron transfer must also exist in the situation in column C, because the excited electron does not thermalize to the lower-level CdS conduction band under direct excitation of the core. By analogy, the barrier to electron delocalization could also be present for tetrapods in which the absence of a shift in emission energy indicates conduction band alignment. The barrier can only exist for one of the carriers, because complete blocking at the interface would result in recombination in the CdS arm, which is spectrally distinct (fig. S8). Noting that our spectroscopy cannot distinguish between conduction and valence band blocking, we follow the earlier assignment of effective hole localization in the core of CdSe/CdS nanoparticles because of a larger offset in the valence band than in the conduction band (*29*). We speculate that the greater effectiveness of hole transfer across the interface as compared to electron transfer could arise from the difference in wave function symmetry of the carrier species, or result from the much larger energy-level offset.

The observation that excitation energies well above the band gap of both CdSe and CdS (that is, at 3.1 eV) do not result in complete thermalization and thus emission at the lowest energy of the system (Fig. 4, column A), which is only observed under direct core excitation, indicates that additional excitation energy does not play a role in electron transfer to the core. The CdS electron therefore cools before the CdSe/CdS interfacial exciton is formed. Our preliminary statistics on the PLE spectra (fig. S9) indicate that excitation energy–dependent emission is much more prominent in class A tetrapods. This observation is again consistent with the implied morphological disorder of the single class B tetrapod structures, because more narrowly defined (class A) energy levels should be more susceptible to band misalignment at the heterojunction.

Single-particle light-harvesting action thus reveals distinct spectroscopic behavior that is masked in the ensemble, providing insight into the uniformity of the quantum confinement and the degree of electronic delocalization across a heterojunction. Morphologies in which the quantum confinement varies within the particle (due to the formation of a CdS bulb around the CdSe core, as observed in nanorods) give rise to a lifting of the spectral signature of well-defined quantum confinement by smearing out excitonic transitions. As shown in the single-paricle spectrally resolved PLE measurements, band misalignment that is more prevalent in morphologically uniform particles (class A) reveals nonthermalized interfacial excitons, which suggest the presence of an intrinsic barrier to electron transfer between CdS and CdSe. Consequently, whereas particle uniformity and the resulting confinement may be desirable in, for example, light-emitting devices, nanoparticles with low symmetry of the confinement potential (that is, with structural variations: class B) are more suited for light-harvesting applications because of a reduced influence of interfacial barriers. The challenge posed to nanoparticle synthesis is to extend shape engineering to morphology control, so as to create samples in which, for example, all particles exhibit class B morphologies.

References and Notes

1. X. Peng *et al.*, *Nature* **404**, 59 (2000).
2. W. U. Huynh, J. J. Dittmer, A. P. Alivisatos, *Science* **295**, 2425 (2002).
3. L. Manna, D. J. Milliron, A. Meisel, E. C. Scher, A. P. Alivisatos, *Nat. Mater.* **2**, 382 (2003).
4. T. Mokari, E. Rothenberg, I. Popov, R. Costi, U. Banin, *Science* **304**, 1787 (2004).
5. D. V. Talapin *et al.*, *Nano Lett.* **7**, 2951 (2007).
6. P. V. Kamat, *J. Phys. Chem. C* **112**, 18737 (2008).
7. A. Pandey, P. Guyot-Sionnest, *Science* **322**, 929 (2008).
8. L. Amirav, A. P. Alivisatos, *J. Phys. Chem. Lett.* **1**, 1051 (2010).
9. Y. Qu *et al.*, *Nano Lett.* **10**, 1941 (2010).
10. M. J. Walter, J. M. Lupton, *Phys. Rev. Lett.* **103**, 167401 (2009).
11. D. Steiner *et al.*, *Nano Lett.* **8**, 2954 (2008).
12. A. Sitt, F. Della Sala, G. Menagen, U. Banin, *Nano Lett.* **9**, 3470 (2009).
13. A. Pandey, P. Guyot-Sionnest, *J. Chem. Phys.* **127**, 104710 (2007).
14. J. Müller *et al.*, *Nano Lett.* **5**, 2044 (2005).
15. S. A. Empedocles, R. Neuhauser, K. Shimizu, M. G. Bawendi, *Adv. Mater.* **11**, 1243 (1999).
16. H. Htoon, P. J. Cox, V. I. Klimov, *Phys. Rev. Lett.* **93**, 187402 (2004).
17. H. Akiyama, M. Yoshita, L. N. Pfeiffer, K. W. West, A. Pinczuk, *Appl. Phys. Lett.* **82**, 379 (2003).
18. T. Ihara *et al.*, *Phys. Rev. Lett.* **99**, 126803 (2007).
19. Y. Chen *et al.*, *Appl. Phys. Lett.* **93**, 053106 (2008).
20. C. Mauser *et al.*, *Phys. Rev. B* **77**, 153303 (2008).
21. E. Yoskovitz, G. Menagen, A. Sitt, E. Lachman, U. Banin, *Nano Lett.* **10**, 3068 (2010).
22. Materials and methods are detailed in supporting material on *Science* Online.
23. A. Efros, M. Rosen, *Annu. Rev. Mater. Sci.* **30**, 475 (2000).
24. T. Vossmeyer *et al.*, *J. Phys. Chem.* **98**, 7665 (1994).
25. M. Saba *et al.*, *Adv. Mater.* **21**, 4942 (2009).
26. J. Planelles, F. Rajadell, J. I. Climente, *J. Phys. Chem. C* **114**, 8337 (2010).
27. R. G. Neuhauser, K. T. Shimizu, W. K. Woo, S. A. Empedocles, M. G. Bawendi, *Phys. Rev. Lett.* **85**, 3301 (2000).
28. A. M. Smith, S. Nie, *Acc. Chem. Res.* **43**, 190 (2010).
29. X. Peng, M. C. Schlamp, A. V. Kadavanich, A. P. Alivisatos, *J. Am. Chem. Soc.* **119**, 7019 (1997).

30. The authors thank K. van Schooten for technical assistance and R. Polson, M. DeLong, and S. Rupich for help with SEM measurements and are indebted to NSF (grants CHE-0748473 and DMR-0213745) and the U.S. Department of Defense Office of Naval Research (grant N00014-10-1-0190). J.M.L. and D.V.T. are fellows of the David and Lucile Packard Foundation.

Supporting Online Material

www.sciencemag.org/cgi/content/full/330/6009/1371/DC1
Materials and Methods
SOM Text
Figs. S1 to S10
Table S1
References

21 September 2010; accepted 3 November 2010
10.1126/science.1198070